APL Materials

RESEARCH ARTICLE | JUNE 08 2020

Aero-ZnS architectures with dual hydrophilic–hydrophobic properties for microfluidic applications

Irina Plesco ; Tudor Braniste ; Niklas Wolff ; Leonid Gorceac ; Viola Duppel; Boris Cinic ; Yogendra Kumar Mishra ; Andrei Sarua ; Rainer Adelung ; Lorenz Kienle ; Ion Tiginyanu

Check for updates

APL Mater. 8, 061105 (2020)
https://doi.org/10.1063/5.0010222

View Online
Export Citation
CrossMark

Articles You May Be Interested In

Mechanical and electrical properties of CdTe tetrapods studied by atomic force microscopy

J. Chem. Phys. (November 2007)

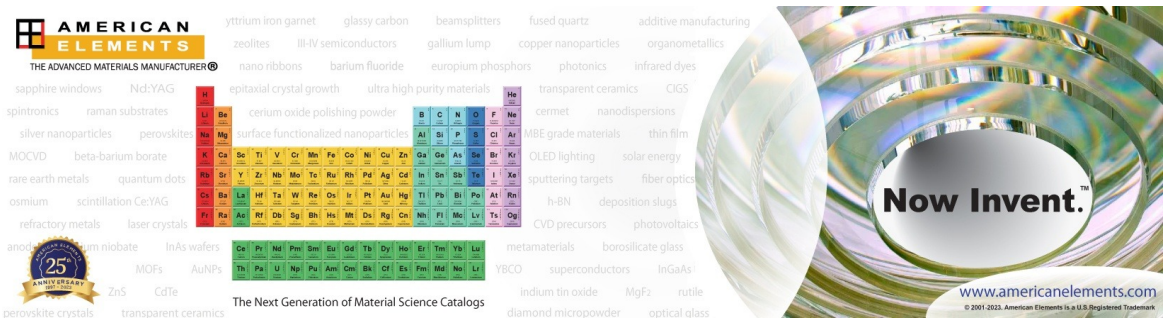
Controlled Growth of CdSe Tetrapod Nanocrystals

AIP Conference Proceedings (April 2007)

Cubatic phase for tetrapods

J. Chem. Phys. (March 2004)

22 September 2023 09:44:19



AIP Publishing

Aero-ZnS architectures with dual hydrophilic–hydrophobic properties for microfluidic applications

Cite as: APL Mater. 8, 061105 (2020); doi: 10.1063/5.0010222
Submitted: 8 April 2020 • Accepted: 21 May 2020 •
Published Online: 8 June 2020

View Online Export Citation CrossMark

Irina Plesco,[1,2,a)] Tudor Braniste,[1] Niklas Wolff,[2] Leonid Gorceac,[3] Viola Duppel,[4] Boris Cinic,[3] Yogendra Kumar Mishra,[5] Andrei Sarua,[6] Rainer Adelung,[2] Lorenz Kienle,[2,a)] and Ion Tiginyanu[1,7,a)]

AFFILIATIONS

[1]National Center for Materials Study and Testing, Technical University of Moldova, Stefan Cel Mare Ave. 168, MD-2004 Chisinau, Republic of Moldova
[2]Institute for Materials Science, Kiel University, Kaiserstrasse 2, D-24143 Kiel, Germany
[3]Department of Physics and Engineering, State University of Moldova, Alexei Mateevici St. 60, MD-2009 Chisinau, Republic of Moldova
[4]Nanochemistry, Max Planck Institute for Solid State Research, Heisenbergstrasse 1, 70569 Stuttgart, Germany
[5]Mads Clausen Institute, NanoSYD, University of Southern Denmark, Alsion 2, 6400 Sønderborg, Denmark
[6]H. H. Wills Physics Laboratory, School of Physics, University of Bristol, Tyndall Avenue, Bristol BS8 1TL, United Kingdom
[7]Academy of Sciences of Moldova, Stefan Cel Mare Ave. 1, MD-2001 Chisinau, Republic of Moldova

[a)]**Authors to whom correspondence should be addressed:** irina.plesco@cnstm.utm.md, lk@tf.uni-kiel.de, and ion.tighineanu@cnstm.utm.md

ABSTRACT

Here, we report on a new aero-material, called aero-ZnS, representing self-organized architectures made of ZnS hollow micro-tetrapod structures with nanoscale thin walls. The fabrication process is based on the hydride vapor phase epitaxy of CdS on sacrificial micro-tetrapods of ZnO with simultaneous or subsequent transformation of CdS into ZnS and removal of the sacrificial ZnO crystals. The nanostructure of the obtained ZnS hollow micro-tetrapods exhibits the polytypic intergrowth of wurtzite- and sphalerite-type phases perpendicular to their close packed planes. The inner surface of the micro-tetrapod walls preserves oxygen sites, as demonstrated by imaging based on electron energy-loss filtering. The self-organized aero-ZnS architecture proves to be hydrophilic under tension and hydrophobic when compressed against water. Self-propelled liquid marbles assembled using ZnS hollow micro-tetrapod structures are demonstrated.

© 2020 Author(s). All article content, except where otherwise noted, is licensed under a Creative Commons Attribution (CC BY) license (http://creativecommons.org/licenses/by/4.0/). https://doi.org/10.1063/5.0010222

INTRODUCTION

Over the last few years, research on a new class of extremely porous and ultra-lightweight nanoarchitectured materials (so called "aero-materials") has demonstrated highly interesting mechanical stability and physical properties to be considered promising for a broad range of technological applications.[1] For instance, carbon-based aero-materials such as graphene aerogels are envisioned for efficient oil/water separation and energy storage/energy conversion, whereas aerographite and graphene foams do serve as backbone materials for the fabrication of hybrid micro-/nano-architectures.[2,3] These foams may find applications in extremely broad-band optical detectors, novel gas sensors, and robust ultra-lightweight pressure sensors.[2–11] Along with this, a sacrificial template approach was demonstrated to synthesize aero-Si and aero-BN foams, which exhibit sensitivity to acetone and ammonia gas or demonstrated highly efficient optical light scattering properties, respectively.[12,13]

Recently, we reported the fabrication of the first aero-material based on the semiconductor compound aero-GaN, which exhibits

22 September 2023 09:44:19

dual hydrophilic/hydrophobic behavior and shows the inherent tendency to the self-organization of constituting components when interacting with water.[14] Furthermore, the network structures show self-healing capabilities, high sensitivity to pressure, and remarkable electromagnetic shielding characteristics.[14–18] We demonstrated the possibility to fabricate a liquid marble (LM) using aero-GaN self-assembling architectures, which represents a drop of liquid covered with GaN hollow micro-tetrapod structures and exhibits self-propelled motion. Aero-GaN exhibits a hydrophobic outer surface due to GaN and a hydrophilic inner surface due to the presence of an ultra-thin layer of ZnO. Placed onto water, the hydrophobic network of hollow tetrapod structures creates a self-supporting shell around the liquid droplet and facilitates the attainment of a high speed of self-propelled rotation of LM, which attains 750 rot min^{-1} when volatile compounds are added to the liquid droplet.[14] The research interest in self-propulsion of liquid marbles is driven by their unique capability to enclose a certain volume of substance keeping gas exchange with external medium and to ensure a constant mixing of the encapsulated liquid.[19,20] Such controllable advection inside the encapsulated droplet is of great importance for small-volume reactions and targeted mass transportation with applications in nano- and biotechnology, synthetic chemistry, microfluidics, and others.[20–27]

Zinc sulfide is an important II–VI semiconductor showing remarkable properties as a wide direct bandgap and luminescence in the visible spectrum, which makes it suitable for various applications including LED technology, lasers, infrared windows, sensors, biodevices, and field emitters.[28–32] Due to the similar chemical and structural properties, the relevance of ZnS may be comparable to the widely known ZnO. ZnS and ZnO crystallize in both cubic sphalerite and hexagonal wurtzite-type structures, the cubic structure in ZnO being metastable.[33,34]

The electronic bandgap in ZnS depends on crystal symmetry (3.72 eV for cubic and 3.77 eV for hexagonal), and it is larger than that of ZnO (3.4 eV for the hexagonal structure).[35,36] The wide bandgap provides ZnS transparency from UV to far IR spectrum, what makes it a good candidate for UV-B and UV-C photodetecting devices and optical windows. At the same time, ZnS is chemically less stable under humid atmosphere with the formation of ZnO and intermediate compounds.[37] Nevertheless, the research interest in ZnS, a classic phosphorescent material, has increased in the last decade due to technological progress in the synthesis of low-dimensional structures, opening new avenues for practical applications, e.g., in ionizing radiation detection, electrochemical immunosensing, and fluorescent biological imaging.[30,31]

The aim of this paper is to elucidate the formation mechanism of ZnS hollow tetrapod structures in a Hydride Vapor Phase Epitaxy (HVPE) process by analyzing the composition and structure of materials at different steps of the technological route. We show that the synthesis of aero-ZnS is possible via the template-assisted growth of thin layers of CdS on ZnO tetrapodal templates with simultaneous or subsequent transformation of CdS into ZnS and further decomposition of the sacrificial core material, leaving three-dimensional hollow tetrapod structures of ZnS. Aero-ZnS is a new 3D aero-material enriching the group of aero-materials with unique structural, electronic, and mechanical properties. We report on its morphologic transformation during the technological process, composition and crystal structure, as well as its dual hydrophilic/hydrophobic behavior disclosed in the network structures.

MATERIALS AND METHODS

The growth process of hollow ZnS tetrapod structures was carried out in a horizontal HVPE reactor with two heating zones. A ZnO micro-tetrapodal network was used as a sacrificial material and Zn source, while CdS powder served as a S source. CdS powder was heated up to 800 °C, and CdS vapors were transported by hydrogen with a flow rate of 160 cm^3 min^{-1} to the second zone maintained at 650 °C/680 °C where the ZnO substrate was placed.[38] The epitaxial process duration was varied between 10 min and 60 min to obtain different wall thicknesses of aero-ZnS. The ZnO tetrapod structures were used as sacrificial substrates, and at the final step of the aero-ZnS preparation, they were dissolved by thermal treatment at 700 °C in H_2 flow with a flow rate of 160 cm^3 min^{-1}. The duration of the substrate removal depends on the thickness of the epitaxial layer and the degree of transformation of CdS into ZnS. Usually, this process takes between 1 h and 2.5 h.

The crystallographic study of the hollow ZnS tetrapod structures was performed on a FEI Tecnai F30 G^2 STwin 300 kV/FEG microscope equipped with an EDX detector (Si/Li, EDAX) a Gatan GIF camera for Electron Energy Loss Spectroscopy (EELS) and Energy Filtered TEM (EFTEM), and a Philips CM30 300 kV/LaB_6 microscope. Electron diffraction and HRTEM image simulations were performed using JEMS electron microscopy simulation software. High-resolution images were simulated by the multislice method for the ZnS sphalerite structure oriented along ZA [110] using a thickness of 6.11 nm, while for the wurtzite structure along ZA [2-1-10] thickness of 5.32 nm was used. In both cases, a defocus of −60 nm corresponding to the experimental conditions was assumed.

Raman scattering measurements of aero-ZnS were performed using a Renishaw inVia spectrometer at room temperature with a 488 nm diode pumped solid state (DPSS) laser having the maximum power of 20 mW. Laser light was focused on the sample using a microscope lens in a spot of about 0.6 μm diameter. The scattered light was analyzed in a backscattering geometry using 2400 grooves/mm grating and a cooled charge-coupled device detector. The spectrometer was calibrated using the known peak values of a bulk Si sample.

RESULTS AND DISCUSSIONS

The presented HVPE synthesis approach comprises two routes, which are dependent on the substrate temperature regime to obtain ZnS hollow tetrapod structures, as sketched in Fig. 1 and experimentally verified by Scanning Electron Microscopy (SEM) observations included in Fig. 2.

The *first* route [Figs. 1(a), 1(b), and 1(d)] describes the direct growth of ZnS onto ZnO substrates at a temperature of 680 °C. At this temperature, the ZnO reduction is more active and the formation of ZnS is more probable than the formation of CdS [Fig. 1(b)]. Due to this fact, the ZnS shell directly grows on ZnO tetrapod structures, and in the final step, a sacrificial ZnO template is dissolved by heating the samples in a H_2 atmosphere at 700 °C. The

22 September 2023 09:44:19

© Author(s) 2020

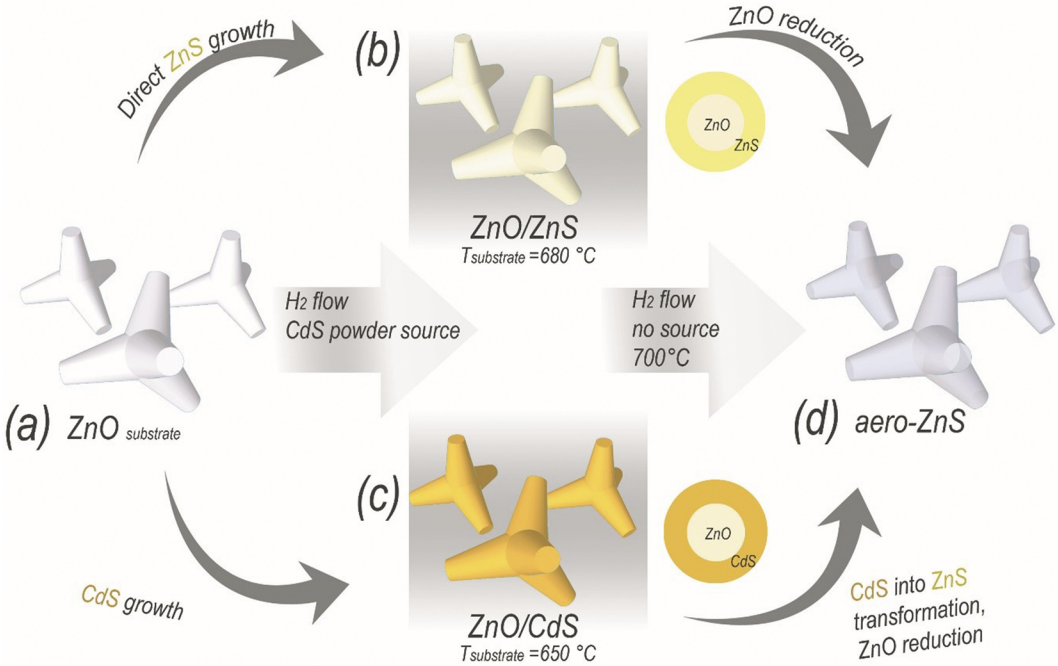


FIG. 1. Schematic representation of the synthesis process of aero-ZnS tetrapod structures: (a) ZnO substrate for the HVPE process, (b) formation of the ZnS epitaxial layer on ZnO, (c) formation of the CdS epitaxial layer on ZnO, and (d) the final aero-ZnS material.

removal of sacrificial ZnO results in the formation of ZnS hollow micro-tetrapod structures, as shown in Figs. 1(d), 2(c), and 2(d). The *second* route [Figs. 1(a), 1(c), and 1(d)] describes the coverage of ZnO substrates by a CdS shell at 650 °C [Figs. 1(c) and 2(b)] and subsequent transformation into ZnS and ZnO reduction during thermal treatment in H_2 at elevated temperatures (Fig. S1).

Each step of the synthesis process is accompanied by characteristic changes of sample color, density, morphology, and chemical

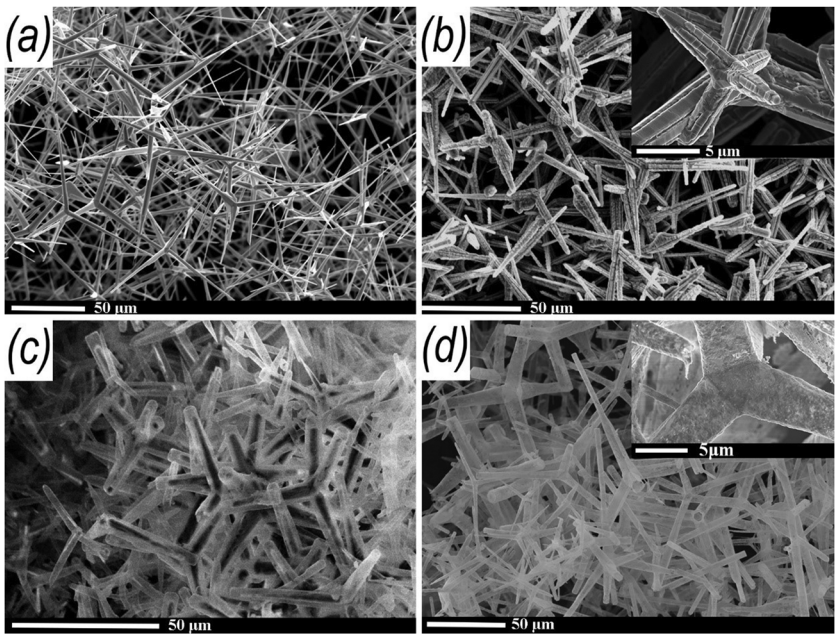


FIG. 2. SEM micrographs of different steps of the aero-ZnS preparation process: (a) ZnO tetrapod structures used as a sacrificial scaffold; (b) ZnO–CdS core–shell structures after the CdS layer were grown in the HVPE process; (c) aero-ZnS obtained after thermal treatment in H_2 flow, residual ZnO can be observed inside hollow structures; and (d) completely hollow aero-ZnS structures.

22 September 2023 09:44:19

© Author(s) 2020

composition. Thus, the initial ZnO tetrapodal template appears white; after the growth of the CdS shell, it turns into intense yellow; and after the transformation of CdS into ZnS, the sample color becomes white again; and the ZnO–ZnS structure displays pale yellow tone. It is notable that during the ZnO scaffold decomposition [Fig. 2(c)], the process starts from the shell to the center. Such behavior can be related to interstices contained in the epitaxial layer through which hydrogen penetrates inside and reduces the scaffold, creating the growing space between shell and scaffold.

Nanowire growth experiments implying co-fed sources containing both Cd^{2+} and Zn^{2+} cations demonstrated that they possess a different reactivity. Thus, in the technological processes implying such a kind of source, core–shell CdS–ZnS or $Cd_xZn_{1-x}S$ compound structures can be obtained.[32,39–41] Using the metalorganic chemical vapor deposition (MOCVD) process at 280 °C or Vapor–Liquid–Solid (VLS) growth at 750–800 °C from the powder mixture of CdS and ZnS, the formation of ZnS or core–shell CdS–ZnS nanowires was demonstrated.[2,41] In the case of core–shell systems, it can be considered that CdS plays a role of the intermediate template in ZnS nanowire formation. Obviously, CdS shows a higher evaporation rate in such a process than ZnS, and the Cd^{2+} cation can be substituted with Zn^{2+}. Notably, the complete conversion of CdS into ZnS can be obtained through the epitaxial process. During the experiments related to aero-ZnS synthesis by means of HVPE, it was observed that 680 °C represents a critical temperature for the decomposition of CdS, leading to the favorable formation of ZnS in the vapor phase. At the conventionally used substrate temperature of 650 °C, we found that CdS can crystallize on the substrate, and in this case, CdS to ZnS transformation occurs during the ZnO scaffold removal at 700 °C. Due to the fact that we use both ZnO and CdS as sources, the kinematics of ZnO reduction will also influence the process. The ZnO tetrapod structures used in our experiments prove to have a high decomposition rate in H_2 at elevated temperatures between 600 °C and 900 °C at H_2 flow rates of 90–160 ml min^{-1}.[15,42]

Residues of Cd and O can be present in the final samples of aero-ZnS obtained via the ZnO template-assisted method with the intermediate stage involving CdS. The detection of ZnO by structural investigations is complicated due to the coincidence of several d-values of both ZnO and ZnS in their wurtzite structure. Chemical analyses by (Scanning) Transmission Electron Microscopy [(S)TEM] Energy-dispersive X-ray spectroscopy (EDX) suggest that the finally prepared samples are composed of Zn, S, and Cd, while Cd concentrations do not exceed 5 at. %. After the thermal treatment of the aero-ZnS material, the formation of highly perforated walls with the thickness of tens of nanometers is evidenced. In this case, EDX can detect only Zn (≈46 at. %) and S (≈54 at. %) [Fig. 3(a) and Fig. S2]. Energy Filtered TEM (EFTEM) analysis [Fig. 3(b)] was performed, which revealed almost homogeneous distribution of oxygen in aero-ZnS thin walls. A higher signal intensity can be observed on the wall edges perpendicular to the viewing plane due to the higher projected thickness of the film.

ZnS may crystallize in cubic sphalerite, hexagonal wurtzite, and cubic rock salt structures. In the bulk state, the most stable polymorph is the sphalerite structure, which can be transformed into wurtzite at temperatures as high as 1020 °C. Nevertheless, the HVPE technique applied in this study reached only temperatures up to 700 °C. It was experimentally demonstrated that nanostructuring opens the possibility to produce both sphalerite and wurtzite polymorphs at low temperature, for instance, recent studies reported on ZnS nanoparticles with the wurtzite structure.[43–46]

To analyze the crystallographic nanostructure, X-Ray Diffraction (XRD) and transmission electron microscopy were performed on the aero-ZnS. XRD revealed the presence of wurtzite and sphalerite ZnS phases on a macroscale for a sample with 1 × 1 × 1 cm^3 dimensions, presented by its diffractogram in Fig. S4. In order to determine how the material structure evolved on the atomic level, HR(TEM) and electron diffraction methods were used. The overview bright-field image of Fig. 4(a) shows a hollow tetrapod arm with porous walls. Precession Electron Diffraction (PED) was performed on the aero-ZnS tube displaying Bragg intensity

22 September 2023 09:44:19

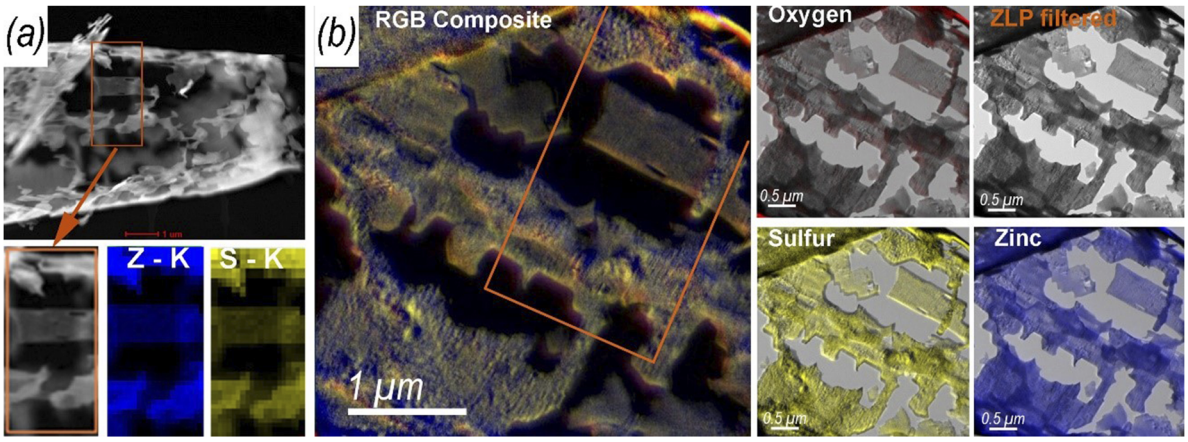


FIG. 3. (a) Top: Z-contrast image of the porous ZnS tetrapod wall and bottom: enlarged section and STEM EDX maps. (b) EFTEM maps, the orange frame marks the same region as in (a), highlighting the presence of oxygen in aero-ZnS.

© Author(s) 2020

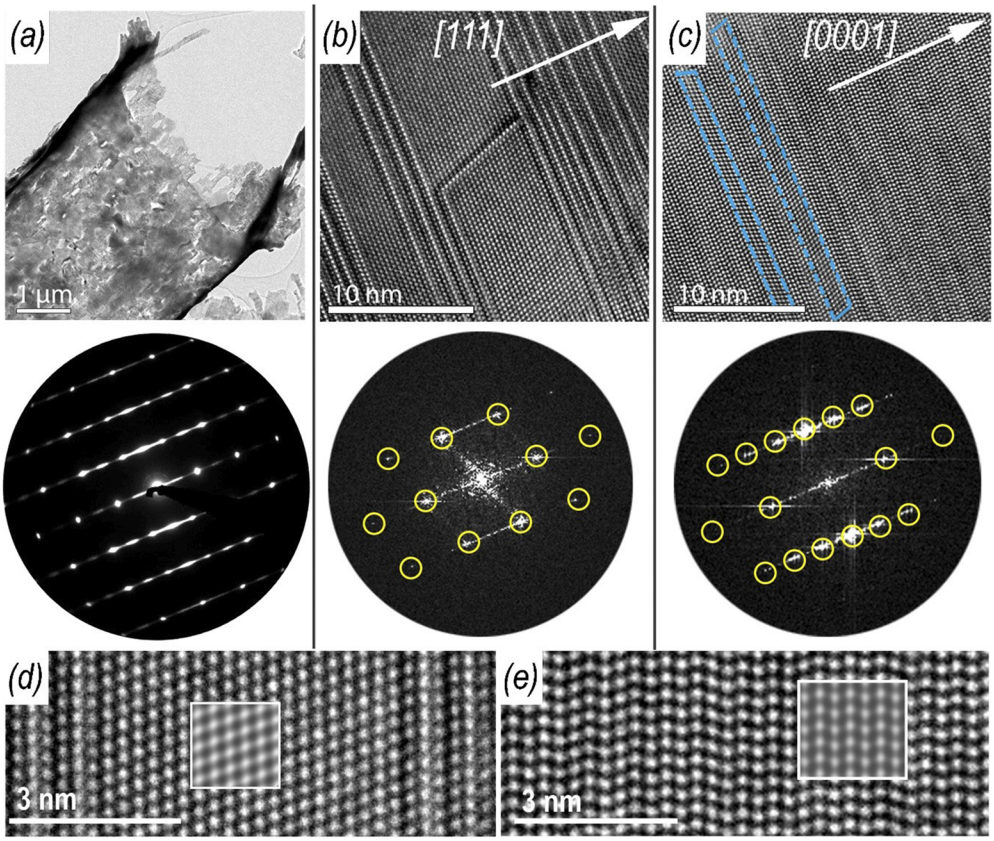


FIG. 4. Crystallographic investigation of aero-ZnS with intergrown domains of wurtzite- and sphalerite-type crystal structures: (a) TEM bright-field image of an aero-ZnS tube and corresponding PED pattern (bottom); (b) HRTEM micrograph and FFT pattern (bottom) showing the [110] pattern of sphalerite-type ZnS, arrow indicates the growth direction; and (c) HRTEM micrograph and FFT pattern showing the [2-1-10] pattern of wurtzite-type ZnS, arrow indicates the growth direction. Inclusions of the cubic motif are marked with blue boxes on the HRTEM micrograph. (d) Magnified region of the sphalerite domain (b) with a phase contrast simulation of the cubic structure as the inset (multislice algorithm) and (e) magnified region of the wurtzite matrix (c) with small cubic motifs and phase contrast simulation of the hexagonal structure as the inset (multislice algorithm).

corresponding to a single crystal of the wurtzite structure in the [2-1-10] zone axis and superimposed diffuse intensity on streaks along the *c*-axis. The diffuse streaks arise from one dimensional disordering, which, in this case, is attributed to the presence of polytypic disordering in the perpendicular direction to the close packed planes of hexagonal and cubic stacking schemes, i.e., (0001) and (111), respectively. Further analysis by HRTEM confirms that the walls of ZnS hollow tetrapods consist of intergrown sphalerite- and wurtzite-type layers. In both cubic and hexagonal structures, Zn and S atoms are tetrahedrally coordinated, but the stacking sequence of close packed atomic layers refers to $(ABC)_n$ and $(AB)_m$, respectively.[47] The HRTEM micrograph [Fig. 4(b)] presents a region of a ZnS thin wall exhibiting a cubic stacking sequence, which is disrupted by numerous basal-plane stacking faults (type I1) perpendicular to the growth direction.[48,49] The formation of basal plane stacking faults can be considered as a wurtzite–sphalerite transition within a few atomic layers. An overall Fast Fourier Transformation (FFT) pattern of the micrograph shown in Fig. 4(b) reveals the ZnS sphalerite structure oriented along ZA [110], as indicated by the yellow circles stemming from the ED pattern simulation. The opposite situation is demonstrated in Fig. 4(c) showing a wurtzite dominant region oriented along ZA [2-1-10] with narrow cubic domains marked inside blue boxes. The FFT resembles the PED pattern showing the ZA [2-1-10] wurtzite with diffuse intensity because of structural disorder induced by the sphalerite ordered domains. It is notable that the synthesis process is accompanied by partial etching of the ZnS tube walls in the *c*-direction, which is demonstrated by the elongated voids apparent in the TEM micrographs (Figs. 3 and 4 and Fig. S3).

The structural polytypism of aero-ZnS is indicated in the measurement of distinct Raman modes as well. The zone-center phonons of a wurtzite-type ZnS single crystal structure can be classified as follows: $\Gamma_{optic} = A_1 + 2B_1 + 2 \times 10^2 + E_1$ and $\Gamma_{acoustic} = A_1 + E_1$ among which A_1, E_1, and E_2 symmetry modes are Raman-active. The sphalerite type zone-center phonons are denoted by $\Gamma_{optic} = A_1 + E + T_2(LO)$ and $\Gamma_{acoustic} = T_2$.[50,51] The first- and second-order Raman modes in sphalerite and wurtzite ZnS have been studied since 1969.[51–56] However, there are still existing ambiguous assignments

22 September 2023 09:44:19

© Author(s) 2020

of the Raman modes for both structures.[57] Another big challenge represents the identification of Raman modes related to wurtzite and sphalerite structures, which have very close frequencies and are more likely indistinguishable in the case of co-existence of both in the same material.

A Raman spectrum acquired from the aero-ZnS tetrapod structures is depicted in Fig. 5 and contains a wide range of peaks, which can be identified as wurtzite and sphalerite modifications of ZnS.[50–57] These data correlate well with the experimental conditions and HRTEM measurements, which disclosed the presence of two crystalline phases in aero-ZnS.

The spectrum is dominated by the first order phonon modes at 348 cm^{-1} corresponding to the A_1(LO) and E_1(LO) phonons of wurtzite-type ZnS with the calculated values of 347 cm^{-1} and 351 cm^{-1}.[50,57] A pronounced peak observed at 334 cm^{-1} can be induced by the surface optical (SO) phonon, also previously reported for rectangular ZnS and GaP nanowires, InN and GaN nanobelts as well as for porous III-V compounds.[50,55,58–62] Modulation in the nanowire growth rate can produce a modulation in the nanowire cross-sectional area along its length and produce the Raman-active SO phonons, for example, during VLS growth.[52]

Raman modes manifesting at 91 cm^{-1}, 297 cm^{-1}, and 513 cm^{-1} at the W critical point and 2[TO]$_X$ mode at 613 cm^{-1} and also acoustic modes at 177 cm^{-1} and 216 cm^{-1} can be uniquely attributed to the sphalerite modification of ZnS.[54,56]

Several multiphonon modes are also observed for aero-ZnS, which can be assigned to both crystal structures presented in the material. A more detailed list of acquired Raman modes and their assignments is presented in Table I. Combination modes show significant broadening due to the complex nanostructured morphology

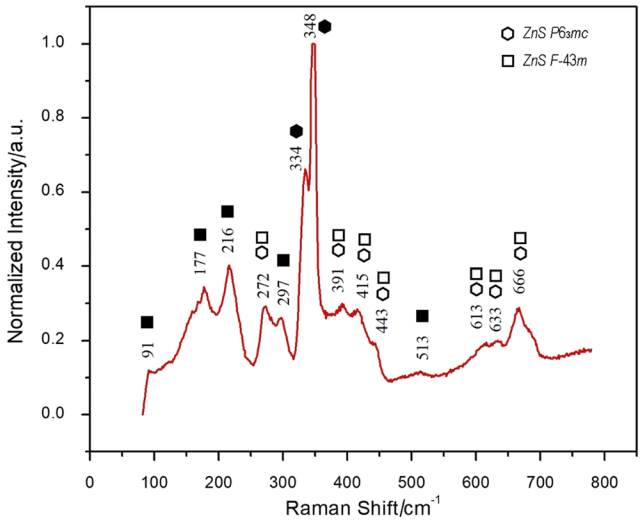


FIG. 5. First- and second-order Raman spectrum of aero-ZnS architectures, measured at room temperature with excitation wavelength 488 nm.

of the aero-material, and a similar change in the spectrum occurs for nanowires and nanocombs.[50]

Nanostructures and particle systems find various applications in electronics and photonics due to the specific modulation of bandgap and electronic transport.[24,32] Recently, the development of self-propelling liquid marbles using micro- and nanoparticles with particular superficial properties was reported, which find

22 September 2023 09:44:19

TABLE I. Raman active modes assignment. Experimental values are shown in boldface.

Uniquely assigned						Common modes for sphalerite and wurtzite structures				
ZnS ***F*-43*m***			ZnS ***P63mc***							
Expt. (***f*, cm^{-1}**)	Calc.[53,55] (***f*, cm^{-1}**)	Assign.	Expt. (***f*, cm^{-1}**)	Calc.[49] (***f*, cm^{-1}**)	Assign.	Expt. (***f*, cm^{-1}**)	Calc. ***F*-43*m***[53] (***f*, cm^{-1}**)	***F*-43*m*** Assign.	Calc. ***P6$_3$mc***[49] (***f*, cm^{-1}**)	***P6$_3$mc*** assign.
1	91[43]	$[LA\text{-}TA_l]_\Sigma$	**334**	332.9	SO	**272**	271	A_1(TO), E_1(TO)	Expt. 275 Calc. 287 Expt. 279 Calc. 288	A_1(TO), E_1(TO)
177	176	$[2TA]_X$	**348**	349.6 352[50]	A_1(LO), E_1(LO)	**391**	394	$[TO + TA]_X$	400	$[TO + TA]_{M\text{–}L\text{–}H}$
216	219	$[2LA]_X$				**415**	416	$[TO + LA]_X$	414, 418	$[LO + TA]_{L,M}$
297	295	2(0) at W				**443**	443	$[LO + LA]_X$	443, 465	$[LO + LA]_{L,M}$
513	511	2(0) at W				**613**	612 608[55]	$2[TO]_X$	610[56]	$2[TO]_{L\text{–}K\text{–}H}$
						633	639	$[LO + TO]_X$	645	$[LO + TO]_{H,M,L}$
						666	665	$2[LO]_\Gamma$	680	$[2LO]_{H\text{–}K}$

© Author(s) 2020

potential applications as microfluidic reactors. In particular, liquid marbles (LM) attract high interest for applications as bioreactors for 3D cell growth, mass transportation, and toxin reduction.[20,63] Liquid marbles are individual droplets of the solution covered with hydrophobic micro- or nanoparticles. The flexible shell has pores that allow the gas outlet from the LM. In previous studies, combinations of nanoparticles with alcohol solutions have been utilized for the preparation of LM. One can mention polytetrafluoroethylene based LM embedding cell culture medium, LM based on Fe_3O_4 nanoparticles embedding H_2O_2 or aqueous solutions of dyes, LM based on Au nanoparticles encapsulating Resazurin alcohol solution, aero-GaN LM with alcoholic solution, and LM based on lycopodium pollen and fumed fluorosilica with aqueous solution of camphor oil.[14,19,20,63] The self-driven locomotion of LM is explained in terms of Marangoni solutocapillary flows and formation of Leidenfrost contact, which lifts LM above the liquid surface with a vapor interlayer. The flexible shell of LM based on micro-/nanoparticles contains pores with micro-/nano-dimensions. The porous shell allows evaporation of the volatile compound from the droplet in different directions with various velocities, leading to Marangoni flows. These asymmetrical flows induce the directed translational motion for marbles with symmetrical shapes or rotational motion for the asymmetrical ones.[14,19] The formation of Marangoni flows and their impact on the self-driven motion of liquids covered in a hydrophobic shell was demonstrated by Bormashenko *et al.* by means of high frequency thermal imaging.[19] It is notable that liquids separated by the LM's shell do not mix and only gas exchange occurs.[64,65]

In the current study for the LM preparation, we used alcohol solution droplets of low and high viscosity covered by hollow ZnS micro-tetrapods, similarly to our previous report.[14] A liquid droplet was placed onto the aero-ZnS tetrapod bed and rolled over to obtain the full coverage of its surface [Figs. 6(a) and 6(c)]. In the process of liquid marble formation, the individual aero-tetrapods touch the water surface with three of their arms, and the process continues until the whole surface of the liquid droplet is covered with ZnS aero-tetrapods. The density of the tetrapods in the network increases, and the aero-ZnS shell becomes mechanically more stable (due to the mutual interpenetration of the tetrapods) after a part of the liquid evaporates and the volume of the liquid marble shrinks. The shell of the liquid marble is characterized by a high degree of porosity determined by the inner diameter of the hollow tetrapod arms (about 2 μm) and the distance between arms of neighboring aero-ZnS tetrapods, which is up to several tens of micrometers. In order to observe the rotational motion of the droplet, it was slightly deformed from spherical geometry and placed on the surface of distilled water [Fig. 6(c)]. The aero-ZnS material demonstrates highly hydrophobic behavior, a drop of water placed on the pressed pill of aero-tetrapod structures discloses a contact angle of 118°, measured by the sessile drop technique [Fig. 6(b)]. While Fig. 6(b) shows the hydrophobic properties of aero-ZnS, the material exhibits hydrophilicity when being removed from the water surface. The detachment force of aero-ZnS from the water surface was estimated by using the following strategy. A sample of aero-ZnS was placed on one arm of two communicating vessels made from glass, while the other arm was used to pour water until it reached the surface of the highly porous aero-ZnS specimen. Subsequently, the water was slowly removed from the free arm using a syringe. Videos 1 and 2 (see the supplementary material) demonstrate how the aero-ZnS specimen holds a 3.3 cm long water column attached to the bottom surface of the aero-ZnS. In the experiment, the liquid was gradually removed from the right arm until it was detached from the bottom surface of the

22 September 2023 09:44:19

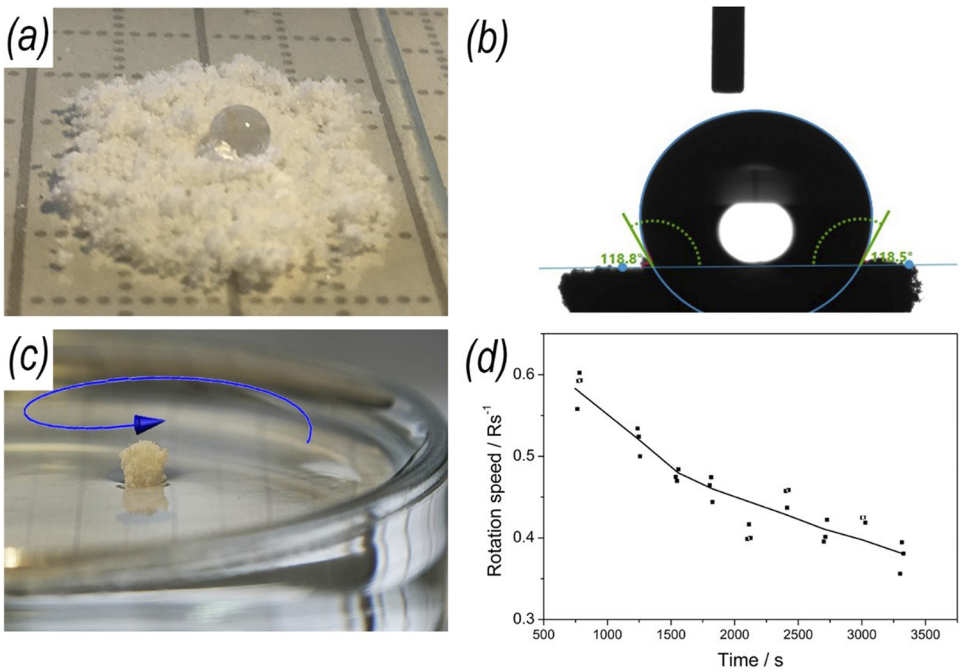


FIG. 6. (a) A water droplet rolling onto an aero-ZnS tetrapod bed, (b) contact angle measurement between a water drop and aero-ZnS surface, (c) a liquid droplet encapsulated by an aero ZnS network on the water surface, and (d) time dependency of speed of rotational motions of the self-propelled aero-ZnS liquid marbles.

© Author(s) 2020

aero-ZnS specimen in the left arm. Taking into account the difference in the water levels at the point of detachment and the inner diameter of communicating glass tubes (33 mm and 4 mm, respectively), the force of detachment was estimated to be as high as 4.03 mN (meaning a specific force or tensile strength of 32 mN cm^{-2}). The LM placed on the distilled water surface immediately starts fast rotational motion. The process of motion was recorded with a high-resolution, high-speed digital camera and further analyzed. The LM's motion on water was investigated during 45 min [Fig. 6(d)]. The maximum angular velocity of an alcohol solution droplet covered by aero-ZnS attained the value of 0.6 rot s^{-1}. During the 45 min time span, the rotation speed dropped down to 0.35 rot s^{-1}. This rotational speed proofs to be about an order of magnitude higher than that inherent to LM based on lycopodium and fluorosilica powder but at the same time is smaller than the rotational speed reported for aero-GaN liquid marbles.[14,19]

After all the liquid from the marbles has been evaporated, the self-assembled structure was contacted with silver paint and the electrical and photoelectrical characterizations in air and vacuum at room temperature have been performed. As shown in Fig. S5, the environment influences upon the electrical and photoelectrical characteristics of the material. In particular, since aero-ZnS is characterized by high specific surface-area, adsorption of gas molecules in air leads to different time dependences of the photocurrent when measured in air and vacuum.

CONCLUSIONS

In conclusion, we developed a new aero-material consisting of hollow ZnS micro-tetrapods obtained by the template assisted approach using HVPE. Two potential synthesis routes have been investigated, and their intermediate stages and the final product, a new form of aero-ZnS material, were examined by SEM and TEM as well as Raman spectroscopy. Elemental analysis of the aero-ZnS material by x-ray spectroscopy and energy-filtered TEM indicated the complete conversion of CdS into a pure phase ZnS material; however, residual oxygen was probed presumably by stemming from a chemically stabilized ultra-thin layer of the ZnO template. Atomic structure observations demonstrated a structural polytypism of wurtzite and sphalerite crystal structures in ZnS. The wurtzite structure is evidenced to be the majority component in aero-ZnS by electron diffraction experiments even though sphalerite is the most energetically favorable modification in the bulk. This observation can be related to the nanoscale phenomenon observed in ZnS nanowires as well. The described aero-ZnS material exhibits an extremely low density of 5.6 mg cm^{-3} and dual hydrophilic/hydrophobic properties, where the outer wall surface demonstrates hydrophobicity, while the inner wall surface demonstrates hydrophilicity. These properties open perspectives for micro-fluidic applications of aero-ZnS, which have been tested on an asymmetrically shaped liquid marble system to achieve rotational motion attaining speeds as high as 0.6 rot s^{-1}.

SUPPLEMENTARY MATERIAL

See the supplementary material for the EDX chemical analysis of different steps of aero-material preparation and the XRD pattern of aero-ZnS, the micrograph and selected area electron diffraction (SAED) showing the direction of the ZnS wall etching, the results of the electrical and photoelectrical characterization of aero-ZnS at room temperature in air and vacuum, and the access links to videos demonstrating the hydrophilicity of aero-ZnS.

ACKNOWLEDGMENTS

I.P., T.B., A.S., and I.T. acknowledge the support from the Ministry of Education, Culture and Research of the Republic of Moldova under Grant No. 20.80009.50007.20 and partial funding from the European Commission under Grant No. 810652, "NanoMedTwin." N.W. and L.K. acknowledge funding from the German Research Foundation under scheme CRC1261 and project A6. I.P. acknowledges support from the DAAD Research Grant (Nos. 57381333 and 91696787). All authors thank Professor Dr. B. Lotsch from the Max Planck Institute for Solid State Research for enabling TEM experiments in her labs.

DATA AVAILABILITY

The data that support the findings of this study are available from the corresponding author upon reasonable request.

REFERENCES

[1] J. Marx, A. Brouschkin, S. Roth, D. Smazna, Y. K. Mishra, H. Wittich, K. Schulte, R. Adelung, and B. Fiedler, Synth. Met. **235**, 145–152 (2018).
[2] Y. Luo, S. Jiang, Q. Xiao, C. Chen, and B. Li, Sci. Rep. **7**, 7162 (2017).
[3] J. Mao, J. Iocozzia, J. Huang, K. Meng, Y. Lai, and Z. Lin, Energy Environ. Sci. **11**, 772–799 (2018).
[4] I. Tiginyanu, L. Ghimpu, J. Gröttrup, V. Postolache, M. Mecklenburg, M. A. Stevens-Kalceff, V. Ursaki, N. Payami, R. Feidenhansl, K. Schulte, R. Adelung, and Y. K. Mishra, Sci. Rep. **6**, 32913 (2016).
[5] L. Ghimpu, O. Lupan, V. Postica, J. Strobel, L. Kienle, M.-I. Terasa, M. Mintken, I. Tiginyanu, J. Marx, B. Fiedler, and R. Adelung, Mater. Sci. Semicond. Process. **100**, 275–282 (2019).
[6] J. Strobel, L. Ghimpu, V. Postica, O. Lupan, M. Zapf, S. Schönherr, R. Röder, C. Ronning, F. Schütt, Y. K. Mishra, I. Tiginyanu, R. Adelung, J. Marx, B. Fiedler, and L. Kienle, Nanotechnology **30**, 065501 (2019).
[7] I. Plesco, J. Strobel, F. Schütt, C. Himcinschi, N. B. Sedrine, T. Monteiro, M. R. Correia, L. Gorceac, B. Cinic, V. Ursaki, J. Marx, B. Fiedler, Y. K. Mishra, L. Kienle, R. Adelung, and I. Tiginyanu, Sci. Rep. **8**, 13880 (2018).
[8] I. Plesco, M. Dragoman, J. Strobel, L. Ghimpu, F. Schütt, A. Dinescu, V. Ursaki, L. Kienle, R. Adelung, and I. Tiginyanu, Superlattices Microstruct. **117**, 418–422 (2018).
[9] M. Dragoman, L. Ghimpu, C. Obreja, A. Dinescu, I. Plesco, D. Dragoman, T. Braniste, and I. Tiginyanu, Nanotechnology **27**, 475203 (2016).
[10] J. Shi, J. Hu, Z. Dai, W. Zhao, P. Liu, L. Zhao, Y. Guo, T. Yang, L. Zou, K. Jiang, H. Li, and Y. Fang, Carbon **123**, 786–793 (2017).
[11] P. Miao, J. Wang, C. Zhang, M. Sun, S. Cheng, and H. Liu, Nano-Micro Lett. **11**, 71 (2019).
[12] I. Hölken, G. Neubüser, V. Postica, L. Bumke, O. Lupan, M. Baum, Y. K. Mishra, L. Kienle, and R. Adelung, ACS Appl. Mater. Interfaces **8**(31), 20491–20498 (2016).
[13] F. Schütt, M. Zapf, S. Signetti, J. Strobel, H. Krüger, R. Roeder, J. Carstensen, N. Wolff, J. Marx, T. Carey, M. Schweichelt, M. Terasa, L. Siebert, H.-K. Hong, S. Kaps, B. Fiedler, Y. K. Mishra, Z. Lee, N. Pugno, L. Kienle, A. Ferrari, F. Torrisi, C. Ronning, and R. Adelung, Nat. Commun. **11**, 1437 (2020).
[14] I. Tiginyanu, T. Braniste, D. Smazna, M. Deng, F. Schütt, A. Schuchardt, M. A. Stevens-Kalceff, S. Raevschi, U. Schürmann, L. Kienle, N. M. Pugno, Y. K. Mishra, and R. Adelung, Nano Energy **56**, 759–769 (2019).

22 September 2023 09:44:19

© Author(s) 2020

[15]M. Dragoman, V. Ciobanu, S. Shree, D. Dragoman, T. Braniste, S. Raevschi, A. Dinescu, A. Sarua, Y. K. Mishra, N. Pugno, R. Adelung, and I. Tiginyanu, Phys. Status Solidi **13**(6), 1900012 (2019).
[16]M. Dragoman, T. Braniste, S. Iordanescu, M. Aldrigo, S. Raevschi, S. Shree, R. Adelung, and I. Tiginyanu, Nanotechnology **30**, 34LT01 (2019).
[17]T. Braniste, S. Zhukov, M. Dragoman, L. Alyabyeva, V. Ciobanu, M. Aldrigo, D. Dragoman, S. Iordanescu, S. Shree, S. Raevschi, R. Adelung, B. Gorshunov, and I. Tiginyanu, Semicond. Sci. Technol. **34**, 12LT02 (2019).
[18]N. Wolff, V. Ciobanu, M. Enachi, M. Kamp, T. Braniste, V. Duppel, S. Shree, S. Raevschi, M. Medina-Sánchez, R. Adelung, O. G. Schmidt, L. Kienle, and I. Tiginyanu, Small **16**, 1905141 (2020).
[19]E. Bormashenko, M. Frenkel, Y. Bormashenko, G. Chaniel, V. Valtsifer, and B. P. Binks, Langmuir **33**(46), 13234–13241 (2017).
[20]X. Han, H. K. Lee, Y. H. Lee, and X. Y. Ling, J. Phys. Chem. Lett. **8**(1), 243–249 (2017).
[21]Y. Sheng, G. Sun, J. Wu, G. Ma, and T. Ngai, Angew. Chem., Int. Ed. **54**(24), 7012 (2015).
[22]R. Abdelaziz, D. Disci-Zayed, M. K. Hedayati, J. H. Pöhls, A. U. Zillohu, B. Erkartal, V. S. K. Chakravadhanula, V. Duppel, L. Kienle, and M. Elbahri, Nat. Commun. **4**, 2400 (2013).
[23]Y. E. Miao, H. K. Lee, W. S. Chew, I. Y. Phang, T. Liu, and X. Y. Ling, Chem. Commun. **50**(44), 5923 (2014).
[24]M. Tebbe, M. Maennel, A. Fery, N. Pazos-Perez, and R. A. Alvarez-Puebla, J. Phys. Chem. C **118**(48), 28095–28100 (2014).
[25]G. Singh, H. Chan, A. Baskin, E. Gelman, N. Repnin, P. Král, and R. Klajn, Science **345**, 1149–1153 (2014).
[26]H. Zhao, D. Wang, C. Gao, H. Liu, L. Han, and Y. Yin, J. Mater. Chem. A **4**, 1366 (2016).
[27]T. Ming, X. Kou, H. Chen, T. Wang, H.-L. Tam, K.-W. Cheah, J.-Y. Chen, and J. Wang, Angew. Chem. **47**(50), 9685 (2008).
[28]J. A. Zapien, Y. Jiang, X. M. Meng, W. Chen, F. C. K. Au, Y. Lifshitz, and S. T. Lee, Appl. Phys. Lett. **84**, 1189 (2004).
[29]S. Okur, N. Üzar, N. Tekgüzel, A. Erol, and M. Çetin Arıkan, Physica E **44**(6), 1103–1107 (2012).
[30]V. S. Kortov, Radiat. Meas. **45**(3), 512–515 (2010).
[31]A. Sharma, V. K. Rao, D. V. Kamboj, R. Gaur, S. Upadhyay, and M. Shaik, Biotechnol. Rep. **6**, 129–136 (2015).
[32]X. Fang, Y. Bando, C. Ye, and D. Golberg, Chem. Commun. **29**, 3048–3050 (2007).
[33]X.-D. Wang, H. Zhou, H.-Q. Wang, F. Ren, X.-H. Chen, H.-H. Zhan, Y.-H. Zhou, and J.-Y. Kang, Chin. Phys. B **24**(9), 097106 (2015).
[34]P. S. Sokolov, A. N. Baranov, Z. V. Dobrokhotov, and V. L. Solozhenko, Russ. Chem. Bull. **59**, 325–328 (2010).
[35]N. Uzar and M. C. Arikan, Bull. Mater. Sci. **34**, 287–292 (2011).
[36]X. Fang, T. Zhai, U. K. Gautam, L. Li, L. Wu, Y. Bando, and D. Golberg, Prog. Mater. Sci. **56**(2), 175–287 (2011).
[37]D. Schultze, U. Steinike, J. Kussin, and U. Kretzschmar, Cryst. Res. Technol. **30**(4), 553 (1995).
[38]Y. K. Mishra, S. Kaps, A. Schuchardt, I. Paulowicz, X. Jin, D. Gedamu, S. Freitag, M. Claus, S. Wille, A. Kovalev, S. N. Gorb, and R. Adelung, Part. Part. Syst. Charact. **30**(9), 775 (2013).
[39]X. Huang, Z. J. Wang, G. Weinberg, X. M. Meng, and M. G. Willinger, Adv. Funct. Mater. **25**(37), 5979 (2015).
[40]Y. J. Hsu, S. Y. Lu, and Y. F. Lin, Adv. Funct. Mater. **15**(8), 1350 (2005).
[41]J. Y. Lee, D. S. Kim, and J. Park, Chem. Mater. **19**, 4663 (2007).
[42]M. Mecklenburg, A. Schuchardt, Y. K. Mishra, S. Kaps, R. Adelung, A. Lotnyk, L. Kienle, and K. Schulte, Adv. Mater. **24**(26), 3437 (2012).
[43]Y. Zhao, Y. Zhang, H. Zhu, G. C. Hadjipanayis, and J. Q. Xiao, J. Am. Chem. Soc. **126**, 6874 (2004).
[44]F. Huang and J. F. Banfield, J. Am. Chem. Soc. **127**(12), 4523–4529 (2005).
[45]J.-Q. Sun, X.-P. Shen, K.-M. Chen, Q. Liu, and W. Liu, Solid State Commun. **147**, 501 (2008).
[46]H. Tong, Y.-J. Zhu, L.-X. Yang, L. Li, L. Zhang, J. Chang, L.-Q. An, and S.-W. Wang, J. Phys. Chem. C **111**, 3893 (2007).
[47]F. A. La Porta, J. Andrés, M. S. Li, J. R. Sambrano, J. A. Varela, and E. Longo, Phys. Chem. Chem. Phys. **16**, 20127–20137 (2014).
[48]Y. Ding and Z. L. Wang, Micron **40**(3), 335–342 (2009).
[49]D. N. Zakharov, Z. Liliental-Weber, B. Wagner, Z. J. Reitmeier, E. A. Preble, and R. F. Davis, Phys. Rev. B **71**, 235334 (2005).
[50]J. H. Kim, H. Rho, J. Kim, Y. J. Choi, and J. G. Park, J. Raman Spectrosc. **43**, 906–910 (2012).
[51]C. A. Arguello, D. L. Rousseau, and S. P. S. Porto, Phys. Rev. **181**, 1351 (1969).
[52]Q. Xiong, J. Wang, O. Reese, L. C. L. Y. Voon, and P. C. Eklund, Nano Lett. **4**(10), 1991–1996 (2004).
[53]O. Brafman and S. S. Mitra, Phys. Rev. **171**, 931 (1968).
[54]W. G. Nilsen, Phys. Rev. **182**, 838 (1969).
[55]J. Schneider and R. D. Kirby, Phys. Rev. B **6**, 1290 (1972).
[56]J. Serrano, A. Cantarero, M. Cardona, N. Garro, R. Lauck, R. E. Tallman, T. M. Ritter, and B. A. Weinstein, Phys. Rev. B **69**, 014301 (2004).
[57]Y. C. Cheng, C. Q. Jin, F. Gao, X. L. Wu, W. Zhong, S. H. Li, and P. K. Chu, J. Appl. Phys. **106**, 123505 (2009).
[58]A. Sarua, J. Monecke, G. Irmer, I. M. Tiginyanu, G. Gärtner, and H. L. Hartnagel, J. Phys.: Condens. Matter **13**, 6687 (2001).
[59]I. M. Tiginyanu, V. V. Ursaki, V. A. Karavanskii, V. N. Sokolov, Y. S. Raptis, and E. Anastassakis, Solid State Commun. **97**, 675 (1996).
[60]I. M. Tiginyanu, C. Schwab, J.-J. Grob, B. Prévot, H. L. Hartnagel, A. Vogt, G. Irmer, and J. Monecke, Appl. Phys. Lett. **71**, 3829 (1997).
[61]I. M. Tiginyanu, G. Irmer, J. Monecke, and H. L. Hartnagel, Phys. Rev. B **55**, 6739 (1997).
[62]I. M. Tiginyanu, G. Irmer, J. Monecke, A. Vogt, and H. L. Hartnagel, Semicond. Sci. Technol. **12**, 491 (1997).
[63]R. K. Vadivelu, C. H. Ooi, R. Q. Yao, J. Tello Velasquez, E. Pastrana, J. Diaz-Nido, F. Lim, J. A. K. Ekberg, N. T. Nguyen, and J. A. St John, Sci. Rep. **5**, 15083 (2015).
[64]E. Bormashenko, Y. Bormashenko, R. Grynyov, H. Aharoni, G. Whyman, and B. P. Binks, J. Phys. Chem. C **119**, 9910–9915 (2015).
[65]G. Lagubeau, M. Le Merrer, C. Clanet, and D. Quéré, Nat. Phys. **7**, 395–398 (2011).

22 September 2023 09:44:19

© Author(s) 2020